EUROPEAN ORGANIZATION FOR NUCLEAR RESEARCH

CERN/EP 79-129
26 October 1979

PRODUCTION OF CHARMED MESONS AND CHARMED BARYONS AT THE ISR

W.M. Geist

CERN, Geneva, Switzerland

1. INTRODUCTION

Although many experiments were dedicated to charm search in hadronic interactions no significant signals were found [1] until recently. This is why no consistent picture for charmed particle production could be extracted from the data so far [2]. After the first observation of D^+ production by the CCHK-Collaboration [3], the obvious aim is to learn more details about the dominant production mechanisms of this new flavour.

The observation of charmed baryon production at the ISR by the CCHK [4] and two other collaborations [5,6] constitutes another major step forward in this field.

Here, the two experiments performed by CCHK with the Split Field Magnet (SFM) will be described, in which charmed meson production and charmed (anti)-baryon production were observed. Cross sections will be presented and consequences of the results will be discussed.

Talk given at the SLAC Summer Institute on Particle Physics,
Stanford, USA, 1979

WMG/ed

2. INCLUSIVE D^+-PRODUCTION AT $\sqrt{s}$ = 53 GeV

2.1 Apparatus and trigger

The experiment was performed at the CERN-ISR using the SFM detector at a c.m. energy $\sqrt{s}$ = 52.5 GeV. The experimental set up (fig. 1) and procedures of data acquisition and analysis have been described in previous publications [7]. The results presented here are based on events obtained by triggering on a negative particle emitted at a c.m. polar angle $\theta \sim 8^0$ with a transverse momentum larger than 0.5 GeV/c (see table 1 for the phase space region covered by the trigger). A threshold Cerenkov counter covering the acceptance of the trigger allowed a separation into "pion" and "non-pion" samples. In the non-pion sample ($\sim$ 100 000 events) about 80% of the triggering particles are K^-, 20% are $\bar{p}$ and the pion contamination is negligible. In the following all triggering particles are treated as kaons and all other particles are assumed to be pions.

2.2 Selection of events

In order to search for resonances in the $K^-\pi^+$ and $K^-\pi^+\pi^+$ systems low multiplicity events with the following structure were selected (fig. 2): a fast (system of) particle(s) was required opposite in rapidity to the $K^-n\pi^+$-system (n = 1, 2) whose transverse momentum is partially balanced locally in rapidity by other particles. Further details and references can be found in [3].

2.3 Mass spectra

In the $K^-\pi^+$ mass distribution from the selected events no structure at the D mass is found, but there is a strong $K^*(890)$ peak (not shown, [3]).

No significant enhancement is found in the $K^-\pi^+\pi^+$ mass distribution at the D mass (fig. 3). To suppress combinatorial background and since it is conceivable that there is a contribution of $\overline{K^*}(890)\pi^+$ to the $K^-\pi^+\pi^+$ final states from D^+ decays the $K^-\pi^+\pi^+$ mass distribution is replotted in fig. 4 for $K^-\pi^+$ systems inside the $K^*(890)$ mass region

(of full width 60 MeV). A pronounced signal is seen in the D mass region; since the $K^-\pi^+\pi^+$ quantum numbers are exotic the signal is not compatible with any non-charmed resonances. In addition, it is concluded from a Monte-Carlo study of position and width of the enhancement that the peak is not a reflection of a known resonance whose decay products have been misidentified.

In order to estimate the significance of the signal and to verify that the signal is not due to kinematics and/or acceptance, three different background spectra have been considered, all obtained from the data with the same selection criteria as used for the $K^-\pi^+\pi^+$ spectrum of fig. 4:

(a) $K^-\pi^-\pi^-$ and $K^-\pi^+\pi^-$ mass distributions.

(b) $K^-\pi^+\pi^+$ mass distributions obtained by combining the K^- from one event with pions from different events ("event mixing").

The background shown in fig. 4 is obtained by adding the background spectra (a), and (b), and by normalizing to the number of $K\pi\pi$ combinations outside the D region.

There are 92 ± 18 events above background in the signal. The D^+ mass was estimated to be 1.91 GeV. The difference of 40 MeV between our estimation and published results is compatible with local systematic errors added to the statistical uncertainty of about 20 MeV. The width of the signal corresponds to the expected mass resolution due to the experimental momentum resolution and to multiple scattering in the beam pipe.

From the number of D^+ events found and assuming equal cross sections for D^+ and D^0 production no significant D^0 signal is expected in the $K^-\pi^+$ mass distribution mentioned above.

From D^+ decays into $\overline{K^{*0}}\pi^+$ one expects about 45% of the $\overline{K^{*0}}$ outside the $\overline{K^{*0}}$ mass cut defined above because of detector resolution. Also from isotropic D^+ decays into $K^-\pi^+\pi^+$ there should be $K^-\pi^+$ mass combinations outside the region 0.866 ÷ 0.926 GeV. In fact D^+ decays with both $K^-\pi^+$ mass combinations outside the K^* region have been found.

2.4 Cross sections

Because of the small number of observed D^+ decays and the sizable D^+ acceptance region (table 1) the inclusive D^+ production cross section inside the acceptance region is model dependent. Cross sections have been calculated with a Monte-Carlo method [3]. With an exponential and a slope parameter of 2 $(GeV/c)^{-1}$ for the transverse momentum dependence of D^+ production the following range of cross sections for the acceptance region Ω was obtained from the measured number of events(*)

$$B \cdot \sigma_\Omega = 1.44\ \mu b \left(\frac{d\sigma}{dx}(D^+) = \text{const.}\right) \div 2.81\ \mu b \left(\frac{d\sigma}{dx} \sim (1 - x)^3\right),$$

with errors of 40%; B is the branching ratio for the decay $D^+ \to \overline{K^{*0}}\pi^+$.

Consequently (sect. 2.3) the cross section for the decay $D^+ \to K^-\pi^+\pi^+$ with one $K^-\pi^+$ combinations in the K^{*0} mass region (0.866 ÷ 0.926 GeV) is

$$B' \cdot \sigma_\Omega = 0.76 \div 1.48\ \mu b.$$

Assuming a 60% $\overline{K^{*0}}$ contribution to D^+ decays into $K^-\pi^+\pi^+$ final states (this is equivalent to assuming that in ∿ 32% of all events there is one $K^-\pi^+$ combination in the above K^* region) one obtains

$$\sigma_\Omega = 53 \div 104\ \mu b.$$

To extrapolate to full phase space it was tried to deduce the longitudinal dependence of the differential D^+ production cross section from published data (fig. 5, see [1] for details).

From ISR measurements of the e/π ratio ($e/\pi \sim 2 \cdot 10^{-4}$, [8]) at small Feynman x one gets

$$\frac{d\sigma}{dy}(D)\Big|_{y=0} \sim 15 \div 30\ \mu b$$

for D production assuming all direct electrons are due to semileptonic D decays. The D^+ data correspond to

---

(*) At most 28 events with D^+ production have been removed from the data by the particular event selection applied. They have been included for the calculation of the cross section.

$$\frac{d\sigma}{dy}(D^+)\Big|_{y\sim 2} \sim 35 \div 66 \ \mu b.$$

These observations suggest that the differential cross section for D production is rather independent of y. A central production mechanism would give

$$\frac{d\sigma}{dy}(D^+)\Big|_{y=0} \gtrsim 200 \ \mu b \text{ or } \frac{e}{\pi} > 15 \cdot 10^{-4} \text{ (from } D^+ \text{ only)}$$

if used to extrapolate from the D^+ data at $y \sim 2$.

Data on inclusive single prompt μ production [9] support this picture: in fig. 6 a prediction from a central production mechanism for the μ/π ratio (curve a) is compared with the data; better agreement with the data is found when using $d\sigma/dy$ = const. for D production (curve b).

This is certainly a rather unexpected shape of the differential cross section for D production and very different from what one could guess from analogy to strangeness production. It therefore needs further experimental confirmation.

The obvious question is now which production mechanism gives rise to such a differential cross section. Two examples are given in fig. 7: In the framework of model I, $\bar{D}$ are produced centrally and fast forward D mesons originate from decays of fast heavy objects (consisting of two valence quarks and a charmed quark) such that $d\sigma/dy(\bar{D}) + d\sigma/dy(D)$ is rather independent of y.

Model II incorporates contributions from central $D\bar{D}$ production and from diffractive N^* production with subsequent N^* decay into $ND\bar{D}$.

For definiteness, model I was used to extrapolate our measurements to full phase space. The following integrated inclusive D^+ cross section was found

$$B \cdot \sigma(D^+) = 6.49 \ \mu b, \text{ or}$$

$$\sigma(D^+) = 240 \ \mu b.$$

Probably $\sigma(D) \sim 2 \cdot \sigma(D^+) = 480 \ \mu b$.

2.5 Comparison with other experiments

To compare the above cross section with results from other measurements all published data have been used to recalculate the corresponding inclusive D cross sections in the framework of model I [1]. The results are given in fig. 8. Inclusive D cross sections are in the range of 8 to 80 μb in the FNAL/SPS energy range, and in the order of 150 to 480 μb at the ISR, with an average of about 300 μb. If a central production mechanism is used to calculate cross sections from the data the resulting values span the range from $\sim$ 20 μb to > 4 mb and at the ISR!

3. INCLUSIVE Λ_c PRODUCTION AT $\sqrt{s}$ = 53 GeV

3.1 Experimental procedure

Continuing the analysis of the data described in sect. 2.3, $K^- p \pi^+$ mass distributions were studied to find evidence for Λ_c production [4]. Again, only the triggering K^- was positively identified. Since a probable diffractive contribution to Λ_c production is even more enhanced by the forward K^- trigger the following cuts were imposed on the events:

(A) Events are accepted when $n_{obs} \leq 11$ (n_{obs} = number of reconstructed tracks, $\bar{n}_{obs} \approx 8$).

(B) Events are accepted only if $|x_{opp}| > 0.5$ or $|x_{opp}| < 0.1$ where x_{opp} is the total reduced longitudinal momentum measured in the hemisphere opposite to the longitudinal direction of the trigger. This cut selects those events in which a leading system is observed opposite in x to the trigger ($|x_{opp}| > .5$) or escapes detection ($|x_{opp}| < .1$), i.e. if a very fast proton stays inside the beam tube or if a fast neutron was produced.

(C) The triggering K^- is required to have reduced longitudinal momentum $x_K > .3$; this is equivalent to a p_T-cut since K^- are only accepted in a small θ range.

(D) Part of the transverse momentum of the Λ_c is required to be compensated locally in rapidity by a "recoiling system". The recoiling system is

defined as the set of particles emitted in the same longitudinal direction as the triggering K^-, but with transverse momentum components k_{Ti} anti-parallel to the transverse momentum of the K^-. Events are accepted if $p_R = \sum_{rec.} k_{Ti} > 0.2$ GeV/c.

(E) The transverse momentum of the $K^-\pi^+p$ system has to be larger than 1 GeV/c.

3.2 Mass spectra

Fig. 9 shows the $K^-\pi^+p$ mass distribution for $K^-\pi^+$ systems in the $K^*(890)$ mass region (.896 ± .040 GeV); the prominent feature is a narrow peak around the Λ_c mass (∿ 2.26 GeV, [10]). To rule out that the signal is due to kinematics and/or acceptance a smooth background obtained by event mixing (sect. 2.2) is also shown. Although the $K^-\pi^+p$ system has non-exotic quantum numbers the narrow width of the signal which is consistent with the experimental resolution renders a possible interpretation as Y^* unlikely. The fact that the width of Λ_c is much smaller than the width of D^+ (sect. 2.3) where the particle taken to be a proton here was assumed to be a pion can be understood as follows: because of the different decay kinematics in the Λ_c and D^+ case the proton from the Λ_c decay is beeing produced at larger rapidities than the pion from the decay $D^+ \to \overline{K^{*0}}\pi^+$. At larger rapidities the momentum resolution (i.e. the resonance mass resolution) is much better in the SFM due to the particular configuration of its magnetic field.

In fig. 10 the $K^-\pi^+p$ mass distribution is displayed for a $p\pi^+$ system in the Δ^{++} mass region (1.236 ± 0.1 GeV). Cut (C) (sect. 3.1) is not used here, but only particles with $x > 0.3$ are taken to be protons; cut D was modified so that only events with $p_R < 0.1$ were removed. A peak in the $K^-\pi^+p$ mass distribution at the Λ_c mass is evident above a smooth background obtained as above by event mixing. This time, however, the background does not seem to describe the mass distribution outside the Λ_c mass very well. In fact, another structure seems to be present.

The width of the $K^-\Delta^{++}$ signal is different from that measured in the $\overline{K^{*0}}p$ case, since due to modified cuts, the decay products populate different regions of phase space.

It was checked that there are no events contributing to the D^+, $\overline{K^{*0}}p$ and $K^-\Delta^{++}$ signals simultaneously.

A preliminary analysis shows that both the $\overline{K^{*0}}$ p and $K^-\Delta^{++}$ final states contribute about 30% to the Λ_c decays into $K^-\pi^+p$.

3.3 Cross sections

The determination of the inclusive Λ_c cross section is model-dependent since the acceptance region (table 1) does not cover full phase space. For simplicity and in analogy to differential cross sections measured for p, n, Λ, Σ^+ production [11] at $x \lesssim 0.6$ it was assumed that $d\sigma/dx(\Lambda_c)$ = const.; an exponential with a slope parameter of 2 $(GeV/c)^{-1}$ was used for the transverse momentum dependence. A Monte-Carlo calculation gives the following cross sections:

$$pp \to \Lambda_c X \quad \hookrightarrow \overline{K^{*0}}p \qquad B \cdot \sigma(\Lambda_c) = 3\ \mu b$$

$$pp \to \Lambda_c X \quad \hookrightarrow K^-\Delta^{++} \qquad B \cdot \sigma(\Lambda_c) = 3.3\ \mu b,$$

(with an error of $\sim$ 40%) not too different from other experiments [5,6]. These cross sections have been corrected for $\overline{K^{*0}}$ and Δ^{++} outside the resonance mass regions defined above (sect. 3.2); they have also been increased by 30% since this is the estimated upper limit of genuine Λ_c events suppressed by cuts A, B, D. With estimated branching ratios $B \approx 7\%$ [12] a Λ_c cross section of about 45 μb is obtained. This seems to be a reasonable value if compared to $\sigma(D^+)$ = 240 μb.

4. PRODUCTION OF $(\bar{\Lambda}_c)$ IN EVENTS WITH AN ELECTRON TRIGGER AT $\sqrt{s}$ = 63 GeV

Since the semileptonic branching ratios for the lightest charmed particles are expected to be fairly large, $e^\pm$ triggers should enrich events with charmed particles produced in pairs, e.g. in the reaction

$$pp \to \Lambda_c \bar{C} X \quad ;$$
$$\Lambda_c \to e^- \quad \text{or} \quad \Lambda_c \to K^- \pi^+ p$$

note that for pair production the charges of the lepton (here e^- from the decay of an anticharmed particle $\bar{C}$) and the charged kaon (here K^- from the Λ_c decay) have the same sign.

4.1 Apparatus and experimental procedure

Also this experiment was performed at the ISR with the upgraded SFM (fig. 11). By rearranging and adding Multiwire Propotional Chambers (MWPC) both acceptance and pattern recognition were improved. The SFM was furthermore equipped with threshold Cerenkov counters, a MWPC with analogue readout (dE/dx chamber) and a time-of-flight system (TOF) to identify particles.

The events were obtained by triggering on $e^{\pm}$ produced at $\theta = 90^0$. This was achieved by requiring a coincidence of signals from two consecutive Cerenkov counters with signals from a road system in the MWPC selecting particle trajectory candidates. Table 2 gives the regions of phase space covered by the trigger.

After track reconstruction the corrected pulse height from the dE/dx chamber was used to separate single electrons from unresolved narrow electron pairs. To further reduce background from non-direct electrons only events with $p_T(e^{\pm}) > 0.4$ GeV/c were retained. In the $p_T(e^{\pm})$ range of $0.4 \div 0.6$ GeV/c most of the electrons from semileptonic D decays are expected.

The pion contribution to the trigger tracks was estimated to be $< 10\%$ on the average and the contamination from non-direct $e^{\pm}$ (not due to charmed particle decays) was calculated to be less than 40%. The present analysis is based on a subsample of the data taken.

4.2 Mass spectra

(a) The event sample with e^- triggers selected according to the procedure outlined above was used to search for resonances in the $K^-p\pi^+$ system. For this study no hadron identification was attempted; the various masses were tentatively assigned to the tracks.

To suppress background some further cuts were applied (see also sect. 3.1)

A': $n_{obs} \leq 14$ ($\bar{n}_{obs} \simeq 15$)

B: as before

F: $x_p, x_K > x_\pi$

G: $|\phi(K\pi p) - \phi(e)| > \pi/2$ and $|y(K\pi p)| > 0.5$.

The resulting $K\pi p$ mass distribution is displayed in fig. 12, a peak at the Λ_c mass is seen above a structureless background from event mixing (sect. 2.3). The insert shows another background obtained from $K^-\pi^+p$ combinations in e^+ trigger events after imposing the above cuts.

Since in this case the signs of the lepton and kaon charges are different, no charm signal should be observed. The absence of a resonance signal in the latter event sample and the fact that the width of the Λ_c resonance in the e^- trigger events is consistent with what is calculated from the detector resolution proves that the enhancement in the non-exotic $K^-\pi^+p$ system is due to a charmed baryon. The contribution of K^* and Δ^{++} resonances to the Λ_c decay into $K^-\pi^+p$ is estimated to be (15 ± 10)% and (25 ± 10)% (preliminary, uncorrected for eventual differences of acceptances). An identical analysis of the $K^+\pi^-\bar{p}$ system produced in events with e^+ triggers does not show any significant signal, i.e. no $\bar{\Lambda}_c$ production is observed in e^+ trigger events.

(b) For a fraction of the events used for the preceeding analysis both $K^\pm$ and $p^{(-)}$ could be identified by TOF. No further kinematic cuts were applied to the data in addition to implicit cuts due to TOF acceptance and TOF resolution. As a consequence the rapidity of the $K\pi p$ systems is confined to $|y(K\pi p)| < 1.0$.

The $K^{+-}p\pi^{-}$ mass distribution for e^{+} trigger events (kaon charge = electron charge) in fig. 13 shows an excess around the $\bar{\Lambda}_c$ mass over a background obtained both from event mixing and from e^{-} trigger events. The width of the peak is again consistent with the detector resolution. This together with the structureless mass distribution from e^{-} trigger events proves that the signal is not generated by acceptance and/or kinematics and that it is due to charmed antibaryons. From fig. 13 one determines a contribution of about (50 ± 30)% from K^{*0} to the $K^{+}\pi^{--}p$ final states from $\bar{\Lambda}_c$ decays (preliminary results).

No indication for Λ_c production is found in a similar analysis of the $K^{-}\pi^{+}p$ system in e^{-} trigger events.

It is clear that calculations of cross sections for $(\bar{\Lambda}_c)$ production in electron trigger events are much more difficult and interesting than in the case of inclusive D^{+} production (sect. 2.4) and inclusive Λ_c production (sect. 3.3) because of the need to:

(a) simulate the performance of all external equipment (C, dE/dx chamber, TOF), and to

(b) study the effects of unknown possible correlations between charmed particles, e.g. in the reactions $pp \to \bar{D}\Lambda_c X$, $pp \to \Lambda_c \bar{\Lambda}_c X$.

5. SUMMARY AND DISCUSSION

After many years of only indirect evidence for charm production in hadron-hadron interactions the first observation of D^{+} production at the ISR may have some important consequences for the understanding of heavy quark dynamics, since:

(a) the inclusive D cross section seems to be much larger than anticipated ($\sigma(D^{+}) \sim 240$ μb, sect. 2.4), and

(b) there are indications that the differential cross section has a rather unusual shape ($d\sigma/dy(D^{+})$ is no strong function of y) with substantial contributions from forward production. These findings should be confirmed experimentally.

Even more recently inclusive production of charmed baryons Λ_c has been measured by our collaboration (and in two other experiments). With a reasonable asssumption for the branching ratios for the decays $\Lambda_c \to \overline{K^{*0}}\, p/K^- \Delta^{++}$ ($B \approx 7\%$) and a differential cross section which is independent of Feynman x, an inclusive cross section of ~ 45 μb is estimated, a reasonable value if compared to $\sigma(D^+) = 240$ μb. This value of the Λ_c cross section, a constant differential cross section $d\sigma/dx$ and a semi-leptonic branching ratio of 10% (like for D mesons) would give a contribution of $\sim 0.3 \cdot 10^{-4}$ to the e/π ratio at small x and $p_T \sim 0.5$ GeV/c.

Preliminary data from SLAC [13] seem to indicate that the branching ratios for $\Lambda_c \to \overline{K^{*0}} p$ and $\Lambda_c \to K^- \Delta^{++}$ are only of the order of 0.5%, which would imply a much larger Λ_c cross section. On the other hand a larger Λ_c cross section would have at least one of the following consequences:

(a) either the semileptonic branching ratio is much smaller than 10%, or

(b) $d\sigma/dx$ has a minimum at small x.

Otherwise the e/π ratio measured at $\sqrt{s} = 53$ GeV to be of the order of $2 \cdot 10^{-4}$ is saturated by Λ_c production alone leaving no room for central D-meson production.

The CCHK data on $\overset{(-)}{\Lambda}_c$ produced in association with triggering leptons open the field for studies of correlations between charmed particles. Already the pattern of observation and non-observation of charmed (anti)-baryons emerging from the above analysis seem to give some hints for particular production mechanisms.

As can be deduced from the procedures by which the signal to background ratios were improved detailed studies of charm production call for a 4π detector, like e.g. the SFM.

I would like to thank all my colleagues from the CCHK (now ACCDHW) Collaboration for their contributions.

REFERENCES

[1] W.M. Geist, CERN/EP 79-78, submitted to the EPS Int. Conf. on High Energy Physics, see refs [2-9, 12-30] given therein.

[2] See, e.g. R. Diebold, Rapporteur's Talk at the 19th Int. Conf. on High Energy Physics, Tokyo (1978).

[3] CCHK Collaboration, D. Drijard et al., Phys. Lett. 81B (1979) 250.

[4] CCHK Collaboration, D. Drijard et al., Phys. Lett. 85B (1979) 452.

[5] ACHMNR Collaboration, K.L. Giboni et al., Phys. Lett. 85B (79) 437.

[6] W. Lockman et al., Phys. Lett. 85B (1979) 443.

[7] CCHK Collaboration, M. Della-Negra et al., Nucl. Phys. B127 (1977) 1;
CCHK collaboration, D. Drijard et al,. CERN/EP/PHYS 78-14, submitted to Nucl. Phys. B;
CCHK Collaboration, M. Della Negra et al., Phys. Lett. 59B (1975) 481.

[8] F.W. Büsser et al., Nucl. Phys. B113 (1976) 189 and Phys. Lett. 53B (1974) 212;
L. Baum et al., Phys. Lett. 60B (1976) 485;
M. Barone et al., Nucl. Phys. B132 (1978) 29.

[9] J.G. Branson et al., Phys. Rev. D20 (1979) 337.

[10] Cazzoli et al., Phys. Rev. Lett. 34 (1975) 1125.

[11] S. Erkan et al., UCLA-1124;
ALN Collaboration, M.M. Block et al., CERN/EP 79-82;
H. Kichimi et al., KEK-Preprint-78-10;
BHM Collaboration, V. Blobel et al., Nucl. Phys. B135 (1978) 379.

[12] J.G. Körner et al., Z. Physik C2 (1979) 117.

[13] B. Richter, Talk given at the SLAC Summer Institute on Particle Physics, Stanford, USA, 1979.

TABLE 1

Acceptance regions for K^-, D^+, Λ_c

Variable	K^-	D^+	Λ_c
x	0.3 - 0.6	0.2 - 0.8	0.4 - 0.8
y	2.0 - 3.0	1.7 - 3.2	2.0 - 2.9
p_T(GeV/c)	> 0.5	> 0.2	> 1.0
$\Delta\phi$	$\sim 70^0$	120^0	100^0

TABLE 2

Kinematic range of $e^{\pm}$ trigger

Variable	Range e^-	Range e^+	Mean e^-	Mean e^+
x	± 0.012	± 0.012	0	0
y	± 0.3	± 0.4	0	0
p_T(GeV/c)	0.3 - 2.0	0.3 - 2.0	0.695	0.672

FIGURE CAPTIONS

Fig. 1 Top view of the Split Field Magnet detector. The shaded area represents the geometrical trigger acceptance, covered by threshold Cerenkov counters.

Fig. 2 Sketch of the event structure (in the rapidity transverse momentum plane) of the selected low multiplicity events.

Fig. 3 $K^-\pi^+\pi^-$ mass distribution for the selected events.

Fig. 4 $K^-\pi^+\pi^+$ mass distributions under the condition that at least one of the two $K^-\pi$ combinations (independent of their charge) has a mass in the K^* region. The broken line represents the background discussed in the text.

Fig. 5 Measured values of the differential cross section $d\sigma/dy$ for D production as derived from measured e/π ratios ($y \sim 0$) and D^+ data ($y \sim 2$). The dashed line shows the extrapolation to $y = 0$ from the D^+ data for a typical central production model.

Fig. 6 Experimental and calculated μ/π ratio as function of Feynman x; contributions from μ pair production were subtracted. Curve (a) gives the prediction from a central production model; curve (b) corresponds to $d\sigma/dy$ (D) = const.

Fig. 7 Diagrams for two models for D production giving rise to a differential cross section $d\sigma/dy$ (D) which is only weakly dependent on y.

Fig. 8 A compilation of cross sections and upper limits for D production calculated with model I (this figure is taken from ref. [1]).

Fig. 9 $K^-p\pi^+$ mass distribution under the condition that the combination $K^-\pi^+$ has a mass in the $K^*(890)$ region. The broken line represents an estimate of the background.

Fig. 10 The $K^-p\pi^+$ mass distribution with $p\pi^+$ in the $\Delta^{++}(1236)$ region. The line is an estimate of the background normalized to the histogram for mass values > 2.5 GeV/c^2.

Fig. 11 Top view of the upgraded SFM, equipped with a TOF system, threshold Cerenkov counters, dE/dx chamber and a LAR calorimeter.

FIGURE CAPTIONS (Cont'd)

Fig. 12 The $K^- p\pi^+$ mass distribution from events with an electron trigger. The broken line is an estimate of the background. The insert shows the $K^- p\pi^+$ mass distribution from events with a positron trigger.

Fig. 13 The $K^+ p\pi^-$ mass distribution for positron triggered events with the K^+ and $\bar{p}$ identified in the time-of-flight system. The broken line represents an estimate of the background. The subset $K^{*0}\bar{p}$ is represented separately.

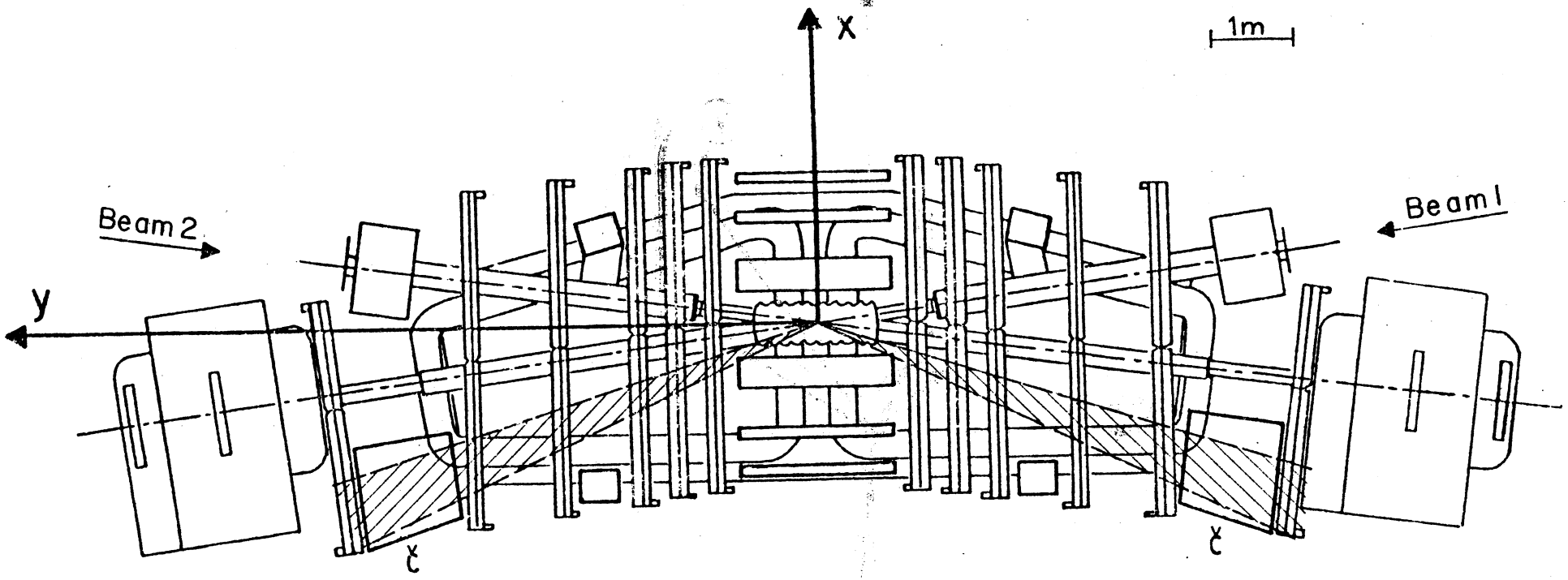

Fig. 1

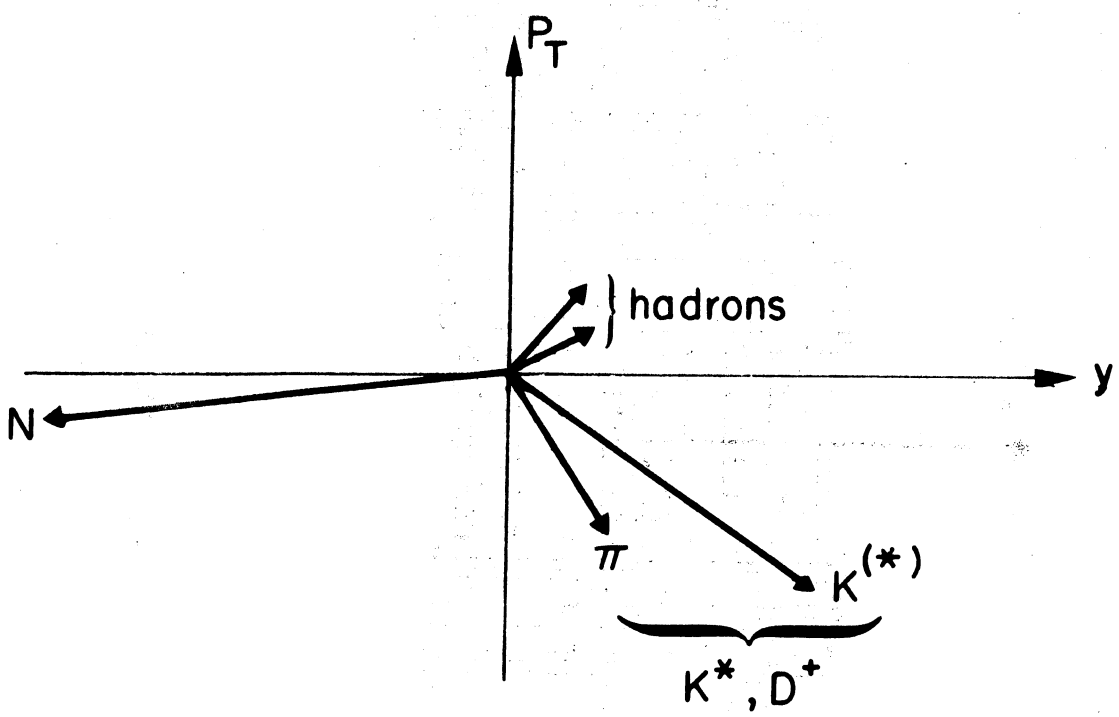

Fig. 2

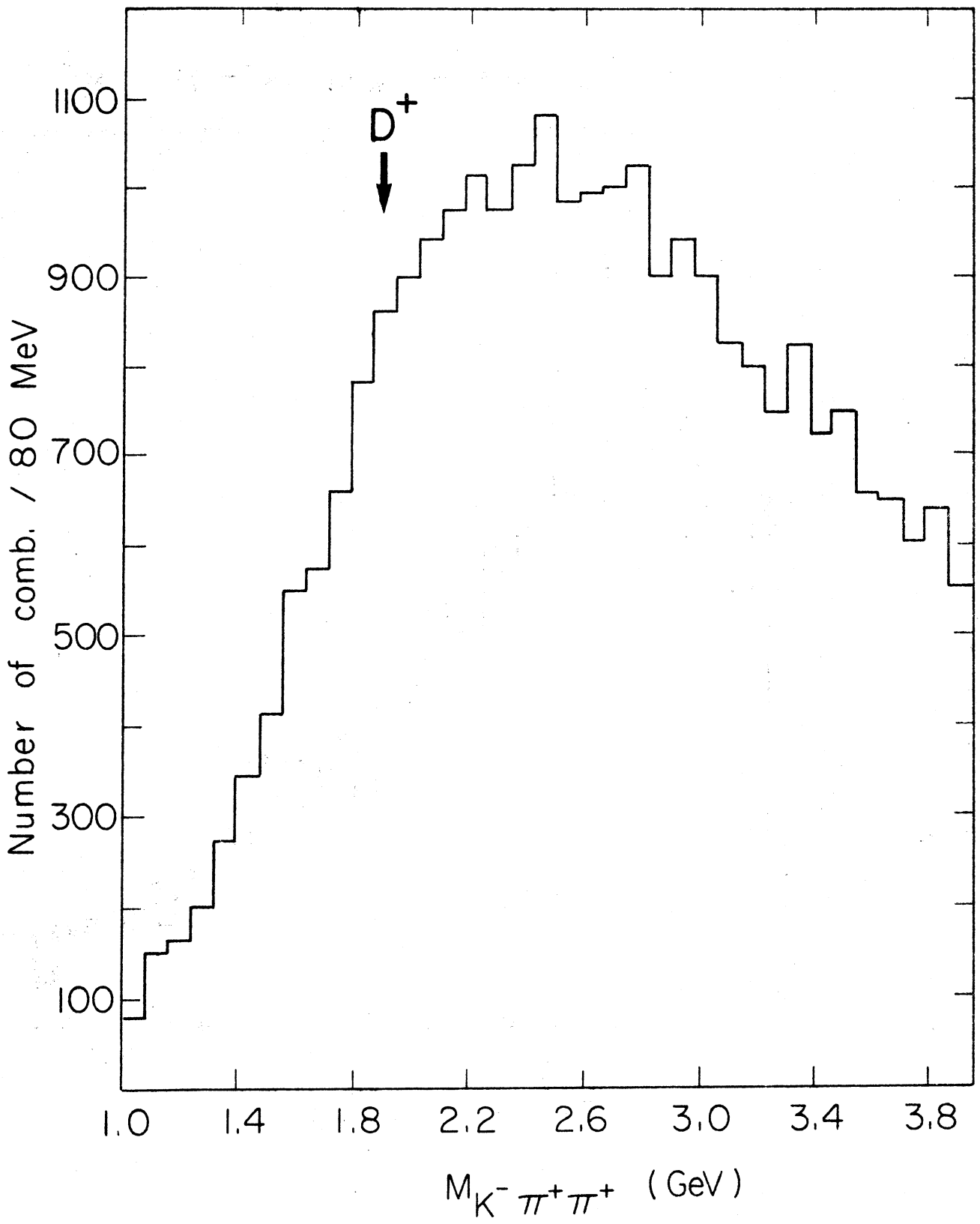
D+
1100
900
700
500
300
100
Number of comb. / 80 MeV
1.0
1.4
1.8
2.2
2.6
3.0
3.4
3.8
M K⁻ π⁺ π⁺ (GeV)

Fig. 3

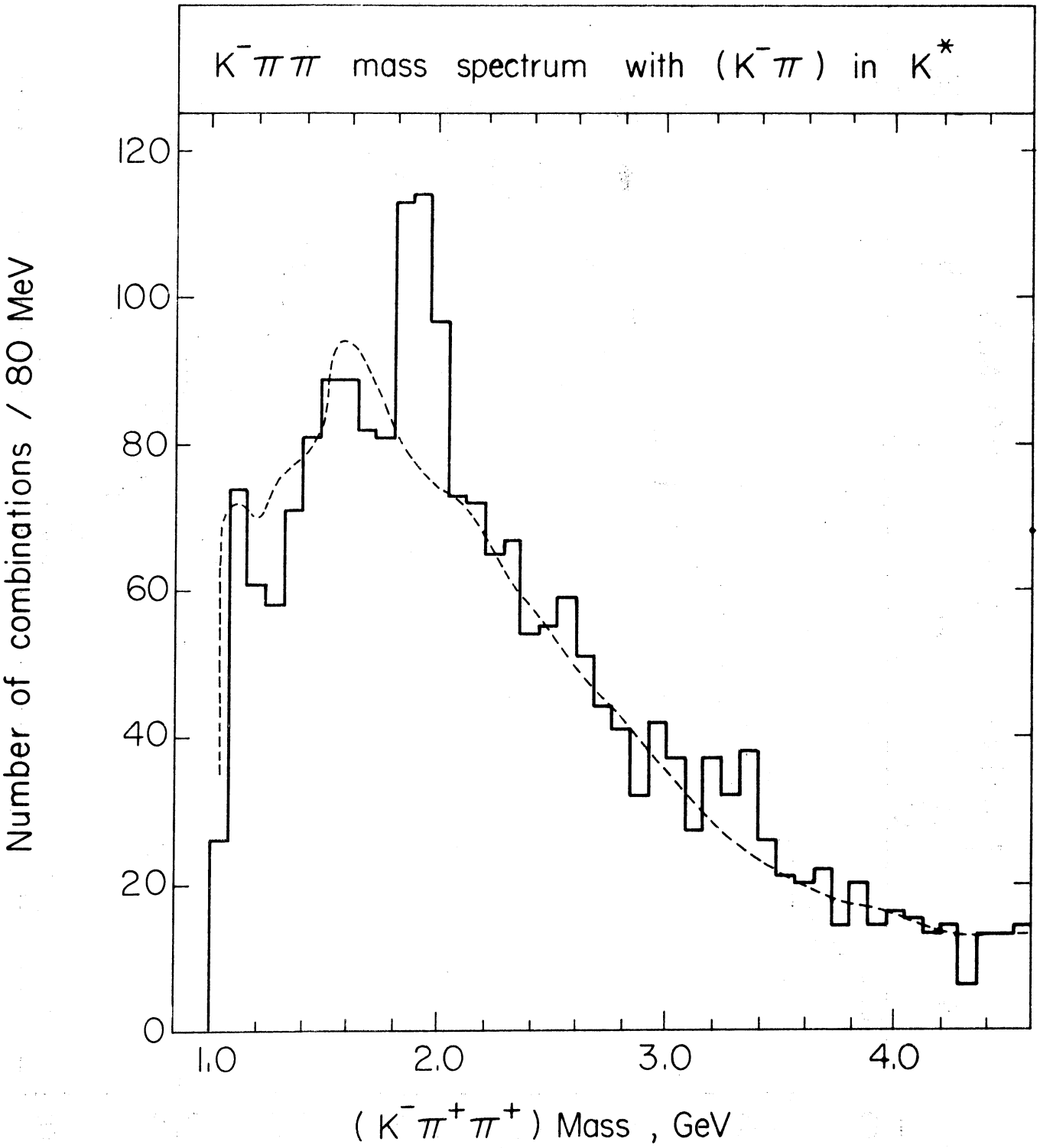
$K^-\pi\pi$ mass spectrum with $(K^-\pi)$ in K^*
Number of combinations / 80 MeV
120
100
80
60
40
20
0
1.0
2.0
3.0
4.0
$(K^-\pi^+\pi^+)$ Mass , GeV

Fig. 4

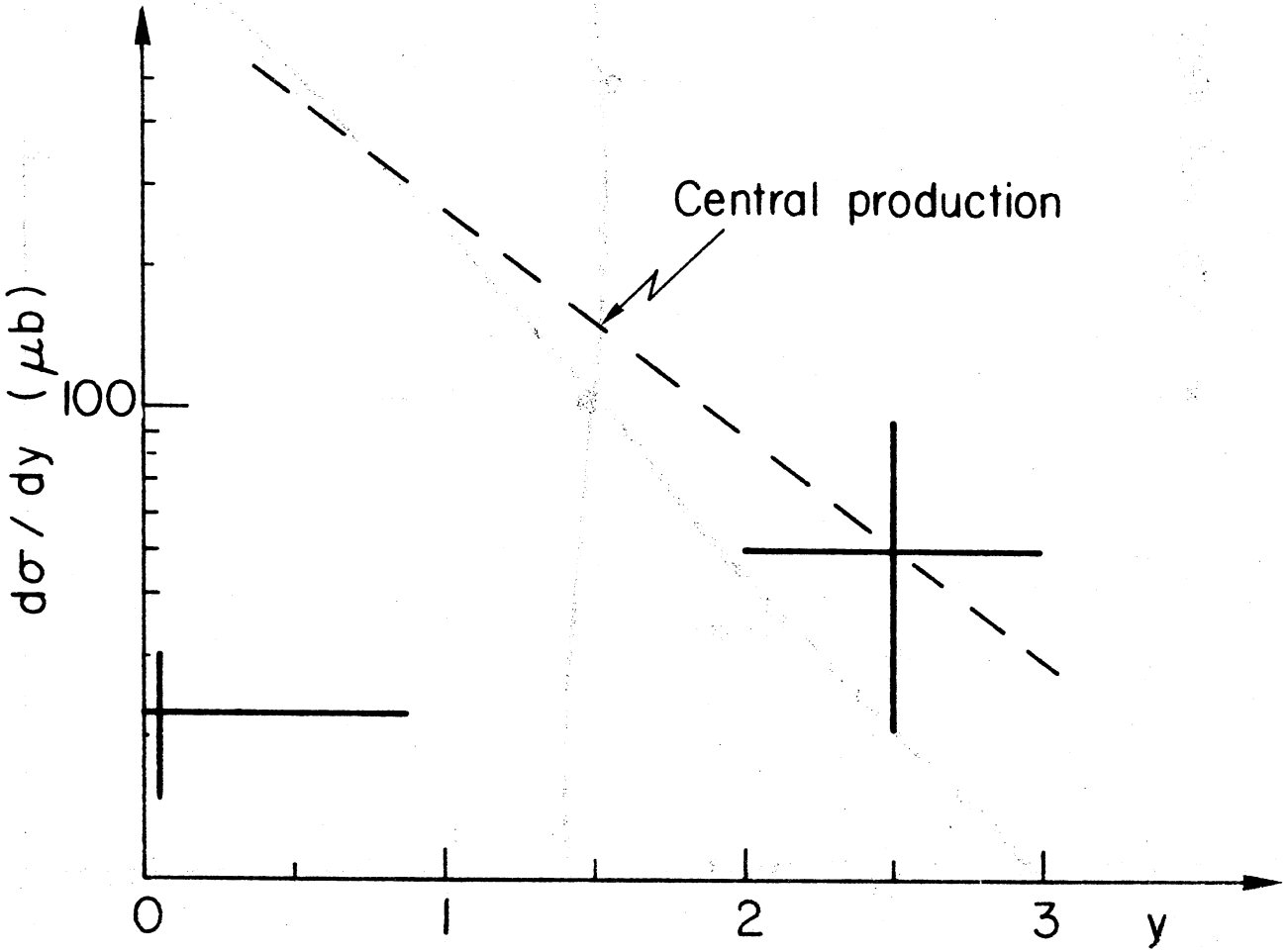

Fig. 5

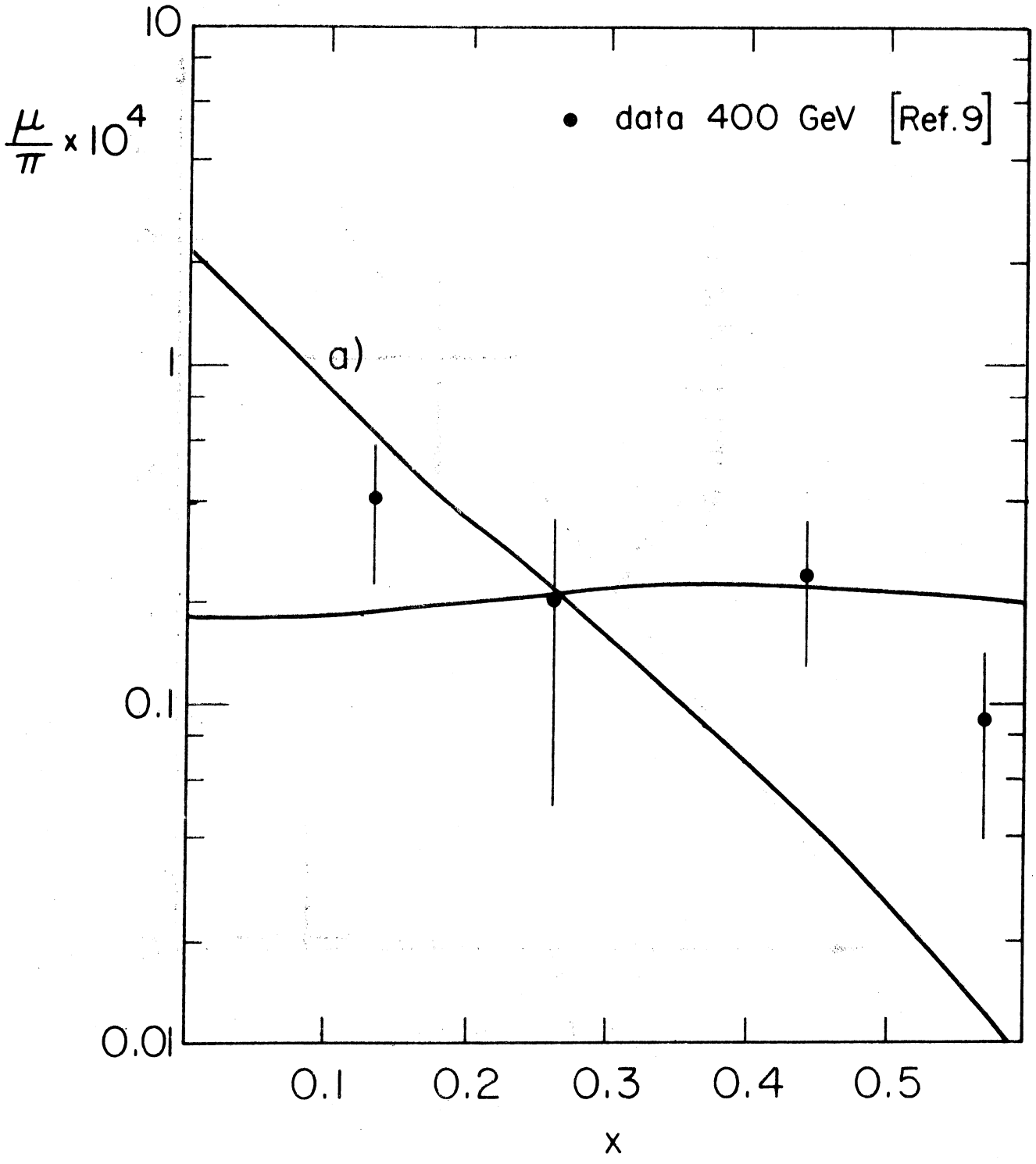
10
1
0.1
0.01
$\frac{\mu}{\pi} \times 10^4$
• data 400 GeV [Ref.9]
a)
0.1
0.2
0.3
0.4
0.5
x

Fig. 6

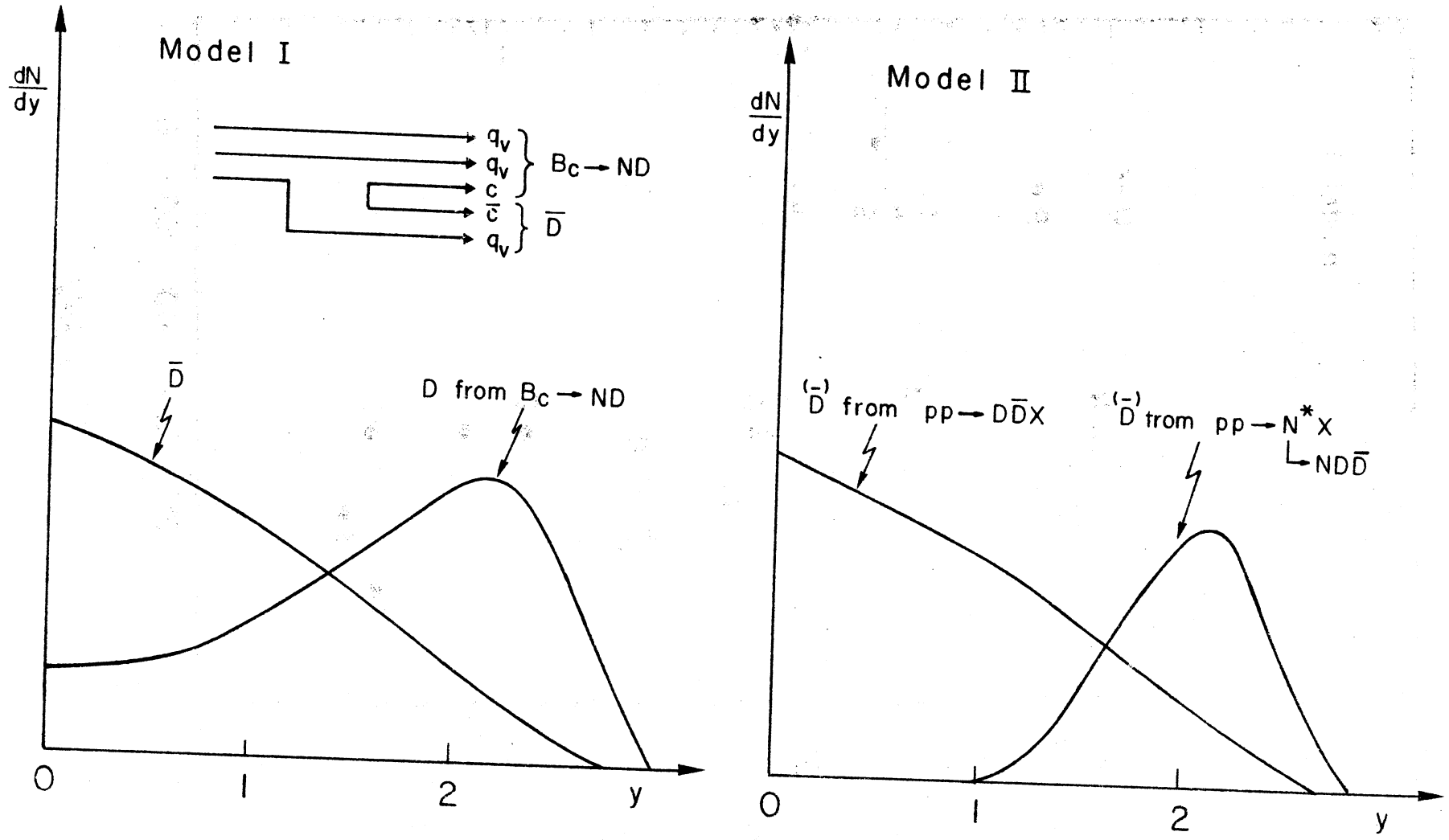
Model I
dN/dy
q_v
q_v
$B_c \to ND$
c
$\bar{c}$
$\bar{D}$
q_v
$\bar{D}$
D from $B_c \to ND$
0
1
2
y
Model II
dN/dy
$\overset{(-)}{D}$ from $pp \to D\bar{D}X$
$\overset{(-)}{D}$ from $pp \to N^*X$
$\hookrightarrow ND\bar{D}$
0
1
2
y

Fig. 7

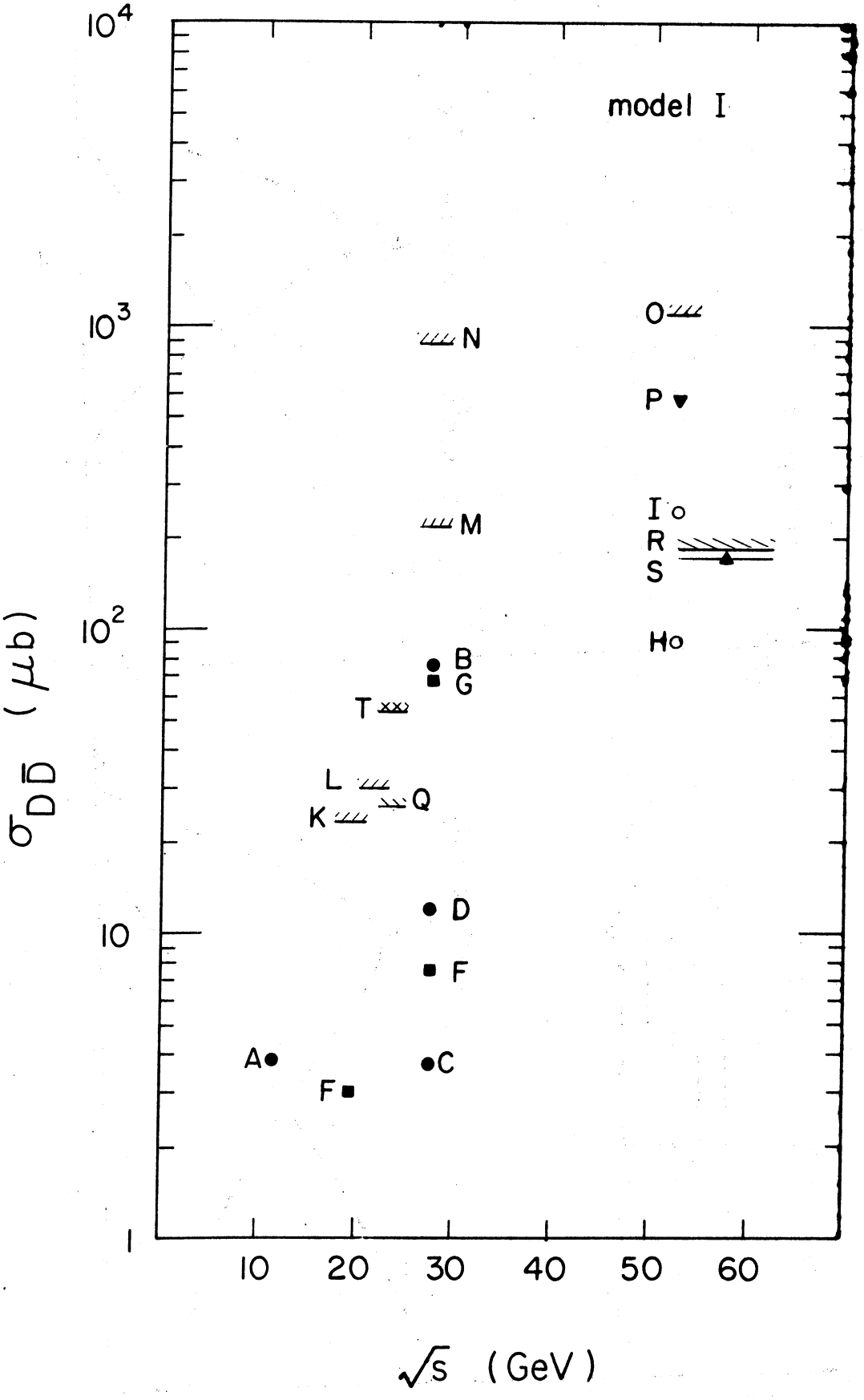
model I
10^4
10^3
10^2
10
1
$\sigma_{D\bar{D}}$ (μb)
10
20
30
40
50
60
$\sqrt{s}$ (GeV)
A
F
C
D
F
B
G
T
L
K
Q
N
M
O
P
I
R
S
Ho

Fig. 8

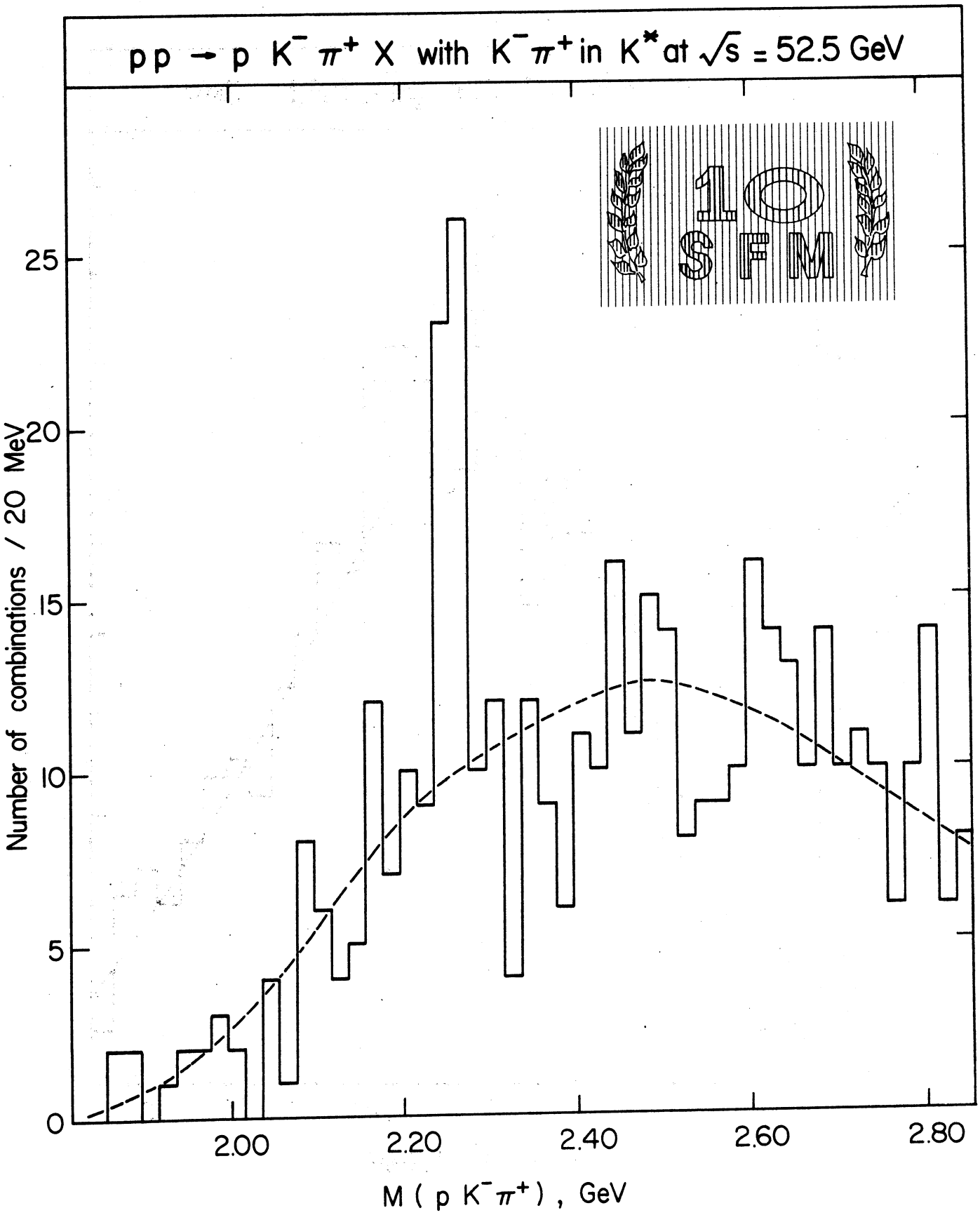
pp → p K⁻π⁺ X with K⁻π⁺ in K* at √s = 52.5 GeV
10 SFM
Number of combinations / 20 MeV
0
5
10
15
20
25
2.00
2.20
2.40
2.60
2.80
M (p K⁻π⁺) , GeV

Fig. 9

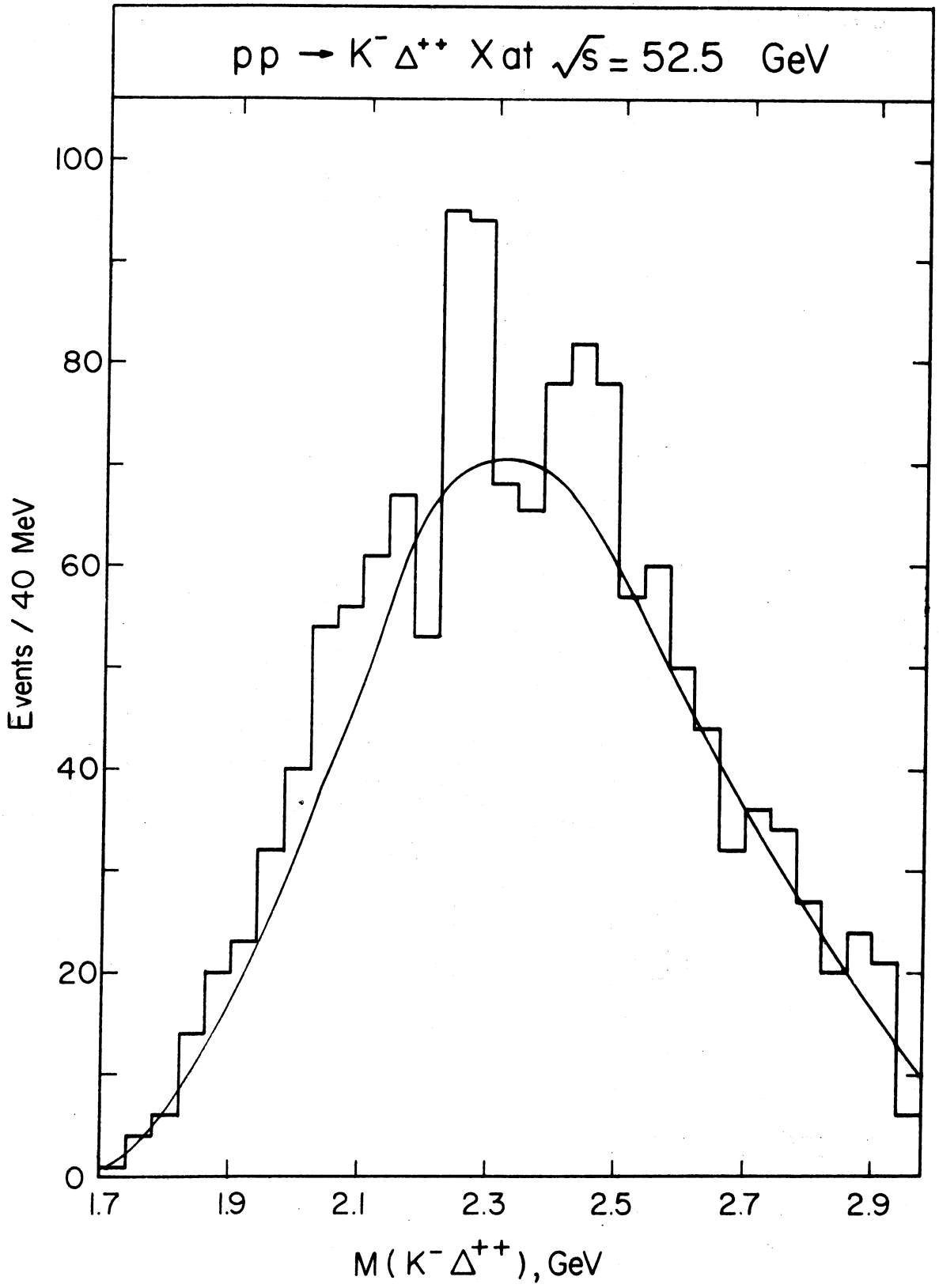
pp → K⁻Δ⁺⁺ X at √s = 52.5 GeV
Events / 40 MeV
0
20
40
60
80
100
1.7
1.9
2.1
2.3
2.5
2.7
2.9
M(K⁻Δ⁺⁺), GeV

Fig. 10

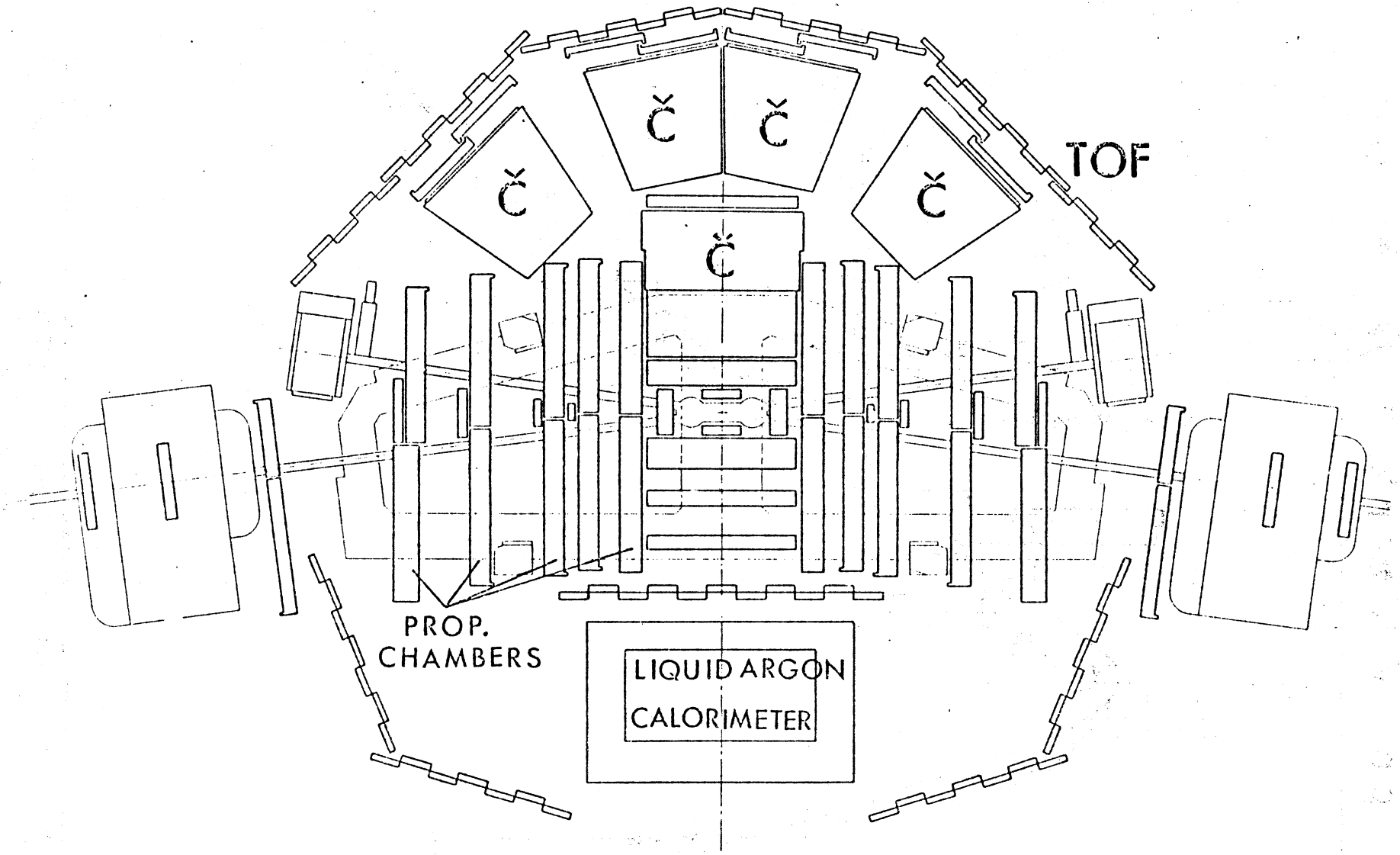

Fig. 11

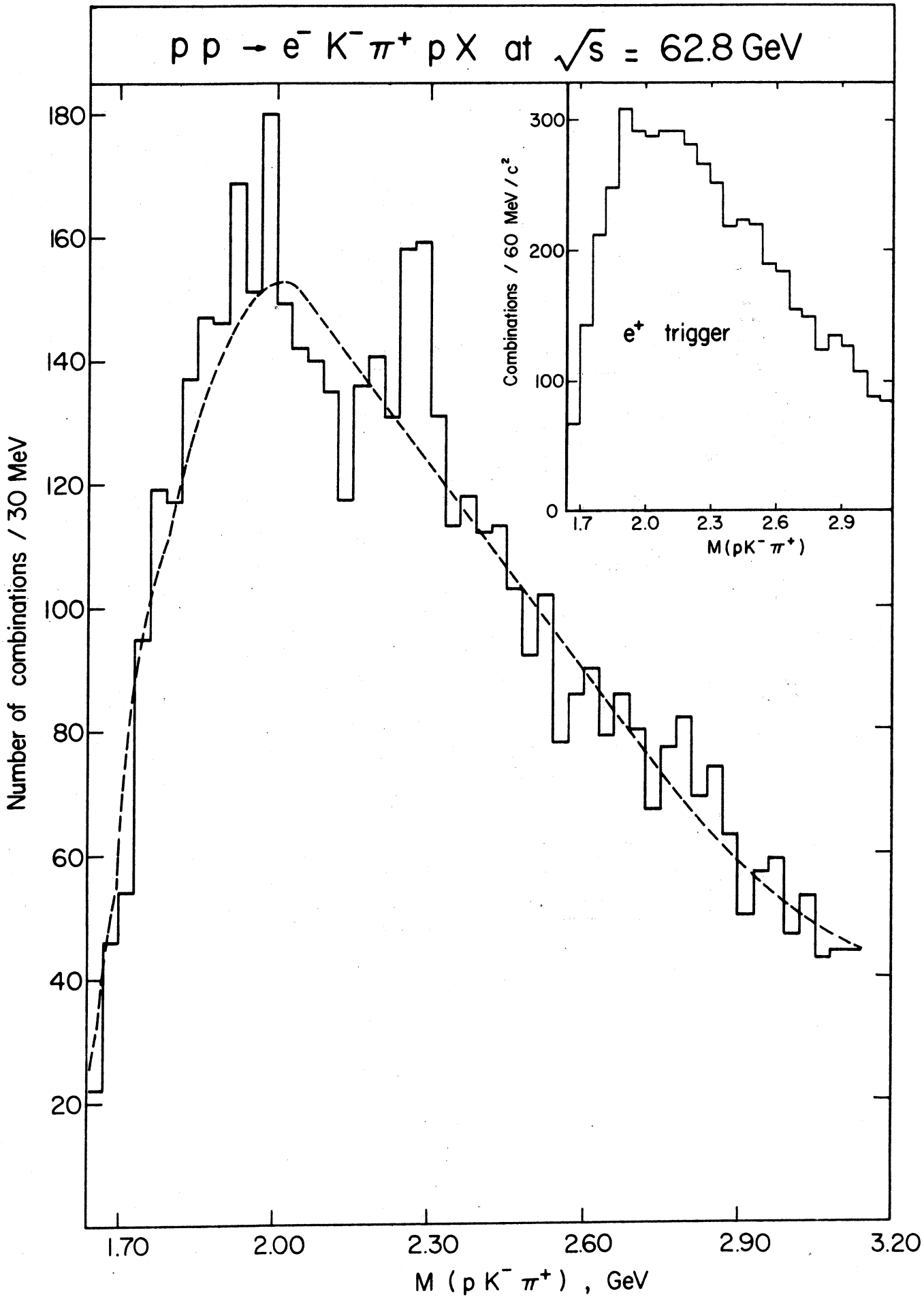
p p → e⁻ K⁻ π⁺ p X at √s = 62.8 GeV
Number of combinations / 30 MeV
M (p K⁻ π⁺) , GeV
Combinations / 60 MeV / c²
e⁺ trigger
M(pK⁻π⁺)

Fig. 12

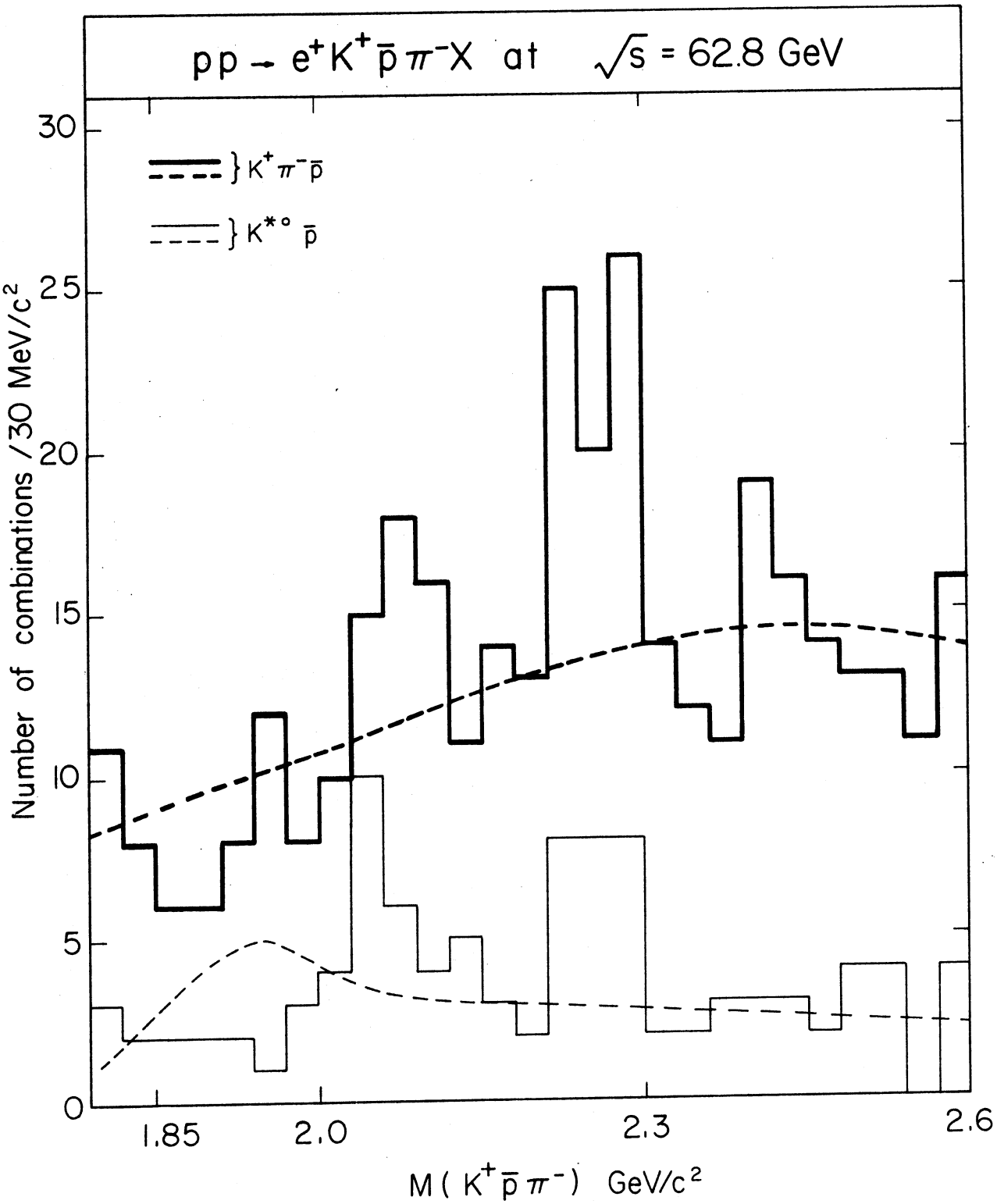
pp → e⁺K⁺p̄π⁻X at √s = 62.8 GeV
} K⁺π⁻p̄
} K*° p̄
Number of combinations /30 MeV/c²
0
5
10
15
20
25
30
1.85
2.0
2.3
2.6
M(K⁺p̄π⁻) GeV/c²

Fig. 13